IL NUOVO CIMENTO **39 C** (2016) 353
DOI 10.1393/ncc/i2016-16353-3

Colloquia: La Thuile 2016

Measurement of the transverse momentum spectrum of the Higgs boson decaying into WW with the CMS experiment

L. Viliani([1])([2])([3]) on behalf of the CMS Collaboration

([1]) *INFN, Sezione di Firenze - Sesto Fiorentino (Firenze), Italy*
([2]) *Università degli Studi di Firenze - Sesto Fiorentino (Firenze), Italy*
([3]) *European Organization for Nuclear Research (CERN) - CH-1211 Genève 23, Switzerland*

received 26 July 2016

Summary. — Differential and integrated fiducial cross sections measured using the Higgs to W^+W^- leptonic decays are presented as a function of the Higgs boson production. The measurements are performed using proton-proton collisions at a centre-of-mass energy of 8 TeV collected by the CMS experiment at the LHC, corresponding to an integrated luminosity of 19.4 fb^{-1}. The Higgs boson transverse momentum is reconstructed using the lepton pair transverse momentum and missing transverse momentum, which originates from the presence of two neutrinos in the final state. The differential cross section is measured as a function of the Higgs boson transverse momentum in a fiducial phase space defined to match the experimental acceptance in terms of the lepton kinematics and event topology. The measurements are compared to theoretical calculations.

1. – Introduction

The discovery of a new boson at the CERN LHC reported by the ATLAS and CMS collaborations in [1,2] has been followed by a comprehensive set of measurements aiming at establishing the properties of the new boson. Measurements reported by ATLAS and CMS are so far consistent with the standard model (SM) expectations for the Higgs boson.

Measurements of the production cross section of the Higgs boson times branching fraction of decay in a restricted part of the phase space (fiducial phase space), together with its kinematic properties, represent an important test for possible deviations from the SM predictions. In particular, it has been shown that the Higgs boson transverse momentum ($p_{\mathrm{T}}^{\mathrm{H}}$) spectrum can be significantly affected by the presence of physics phenomena not predicted by the SM [3]. These measurements also facilitate to test the theoretical predictions in the SM Higgs sector, which provide calculations up to next-to-next-to-leading-order (NNLO) accuracy in perturbative QCD, up to next-to-next-to-leading-logarithmic (NNLL) accuracy in the resummation of soft-gluon effects at small

transverse momenta, and up to next-to-leading-order (NLO) accuracy in perturbative electroweak corrections [4].

Measurements of the fiducial cross sections and of several differential distributions using the 8 TeV LHC data have been reported by CMS in refs. [5, 6] for the $H \to ZZ \to 4\ell$ ($\ell = e, \mu$) and $H \to \gamma\gamma$ decay channels. Here, we report a measurement of the integrated fiducial cross section times branching fraction ($\sigma \times B$) and transverse momentum spectrum for the Higgs boson production in $H \to W^+W^- \to e^\pm\mu^\mp\nu\nu$ decays, based on $\sqrt{s} = 8$ TeV LHC data [7]. The $H \to WW \to 2\ell 2\nu$ channel is characterized by a lower resolution in the p_T^H measurement compared to $H \to \gamma\gamma$ and $H \to ZZ \to 4\ell$ channels because of neutrinos in the final state. However this channel has a significantly larger $\sigma \times B$, exceeding that for the $H \to \gamma\gamma$ by a factor of 10 and $H \to ZZ \to 4\ell$ by a factor of 85 for a Higgs boson mass of 125 GeV, and is characterized by a good signal sensitivity. The sizeable contribution of backgrounds containing a same-flavour lepton pair originating from the Z boson decay is suppressed by looking at different flavour leptons in the final state.

The measurement is performed in a fiducial phase space that closely match the experimental event selection in terms of lepton kinematics and event topology. The effect of the limited detector resolution, as well as the selection efficiency with respect to the fiducial phase space, are corrected to the particle level with an unfolding procedure.

The analysis presented here is based on the previously published $H \to WW \to 2\ell 2\nu$ measurements by CMS [8]. A noticeable difference from those measurements is that this analysis is inclusive in the number of jets, which allows to reduce the uncertainties related to the theoretical modelling of additional jets produced in association with the Higgs boson. The main background contributions arise from two processes: for Higgs p_T values below approximately 50 GeV the dominant background is WW production, while above 50 GeV $t\bar{t}$ pair production dominates.

2. – Data and simulated samples

The analysis makes use of data recorded by the CMS experiment during 2012 and correspond to an integrated luminosity of 19.4 fb^{-1} at a centre-of-mass energy of 8 TeV. The events used in this analysis are triggered by requiring the presence of either one or a combination of electron and muon with high p_T and tight identification and isolation criteria. Single-lepton triggers are characterized by p_T thresholds varying from 17 to 27 GeV for electrons and from 17 to 24 GeV for muons. Dilepton $e\mu$ triggers are required to have one electron or one muon with $p_T > 17$ GeV and the other muon or electron with $p_T > 8$ GeV.

Simulations of the Higgs boson production through the gluon fusion (ggH) and vector boson fusion (VBF) mechanisms are performed using the POWHEG V1 [9] generator, which provides a NLO accuracy calculation in perturbative QCD.

The main background processes, nonresonant $q\bar{q} \to W^+W^-$ and $t\bar{t}$+jets, are simulated using the MADGRAPH 5.1.3 [10] and POWHEG V1 event generators, respectively. The same Monte Carlo (MC) programs are used to simulate other minor background processes. All signal and background generators are interfaced to PYTHIA 6 [11] to simulate the effects of the parton shower, multiple parton interactions, and hadronization. The samples are processed using a simulation of the CMS detector response, as modeled by GEANT4.

3. – Analysis strategy

The basic requirement for the analysis selection consists in two isolated leptons with opposite charge, an electron and a muon, with p_{T} greater than 20 (10) GeV for the leading (subleading) lepton, and with $|\eta| < 2.5$ ($|\eta| < 2.4$) for electrons (muons). No additional electron or muon with $p_{\mathrm{T}} > 10\,\mathrm{GeV}$ is allowed. The two leptons must originate from a single primary vertex, that is, among the vertices identified in the event, the one with the largest $\sum p_{\mathrm{T}}^2$, where the sum runs over all tracks associated with the vertex. The invariant mass of the two leptons, $m_{\ell\ell}$, is required to be greater than 12 GeV. A *projected* $E_{\mathrm{T}}^{\mathrm{miss}}$ variable is defined as the component of $\vec{E}_{\mathrm{T}}^{\mathrm{miss}}$ transverse to the nearest lepton if the lepton is situated within the azimuthal angular window of $\pm\pi/2$ from the $\vec{E}_{\mathrm{T}}^{\mathrm{miss}}$ direction, or the $E_{\mathrm{T}}^{\mathrm{miss}}$ itself otherwise. Since the $E_{\mathrm{T}}^{\mathrm{miss}}$ resolution is degraded by the additional pp interactions per bunch-crossing (pileup), the minimum of two projected $E_{\mathrm{T}}^{\mathrm{miss}}$ variables is used ($E_{\mathrm{T}}^{\mathrm{miss}\angle}$): one constructed from all identified particles (full $E_{\mathrm{T}}^{\mathrm{miss}}$), and another constructed from the charged particles only (track $E_{\mathrm{T}}^{\mathrm{miss}}$). The minimum $E_{\mathrm{T}}^{\mathrm{miss}}$ and $E_{\mathrm{T}}^{\mathrm{miss}\angle}$ for the events are required to be 20 GeV. $Z/\gamma^* \to \tau^+\tau^-$ events are suppressed requiring the vector p_{T} sum of the two leptons, $p_{\mathrm{T}}^{\ell\ell}$, to be greater than 30 GeV and the minimum transverse mass of the lepton pair and the $E_{\mathrm{T}}^{\mathrm{miss}}$ vectors to be greater than 60 GeV. The transverse mass is defined as $m_{\mathrm{T}} = \sqrt{2p_{\mathrm{T}}^{\ell\ell}E_{\mathrm{T}}^{\mathrm{miss}}(1-\cos\Delta\phi(\ell\ell,\vec{E}_{\mathrm{T}}^{\mathrm{miss}}))}$, where $\Delta\phi(\ell\ell,\vec{E}_{\mathrm{T}}^{\mathrm{miss}})$ is the azimuthal angle between the dilepton momentum and $\vec{E}_{\mathrm{T}}^{\mathrm{miss}}$.

Events surviving these requirements are dominantly the ones where a top-antitop quark pair is produced and both quarks decay leptonically (dileptonic $\mathrm{t\bar{t}}$). These events are classified using a combination of b tagging algorithms and rejected requiring to have no jets with $p_{\mathrm{T}} > 30\,\mathrm{GeV}$ identified by the algorithms. Events containing jets with $15 < p_{\mathrm{T}} < 30\,\mathrm{GeV}$ are also rejected if containing a b-tagged jet. In this latter category a soft-muon veto is applied, rejecting the events containing a nonisolated low p_{T} muon, that is likely coming from a b hadron decay.

The overall number of signal events after these requirements is 382, according to the SM expectation.

The fiducial phase space requirements have been chosen to closely match the analysis event selection in order to minimize the dependence of the measurements on the underlying model of the Higgs boson properties and its production mechanism.

The leptons are defined as Born-level leptons, *i.e.* before the emission of final state radiation (FSR), and are required to not come from leptonic τ decays. The effect of including FSR was evaluated to be of the order of 5%. The requirements for the fiducial phase space definition are summarized in table I.

Experimentally, the Higgs boson transverse momentum is reconstructed as the vector sum of the lepton momenta in the transverse plane and $E_{\mathrm{T}}^{\mathrm{miss}}$:

$$\vec{p}_{\mathrm{T}}^{\,\mathrm{H}} = \vec{p}_{\mathrm{T}}^{\,\ell\ell} + \vec{E}_{\mathrm{T}}^{\,\mathrm{miss}}. \tag{1}$$

This analysis has to cope with the limited resolution due to the $E_{\mathrm{T}}^{\mathrm{miss}}$ entering the transverse momentum measurement. The choice of the binning in the transverse momentum spectrum needs to be done taking into account the detector resolution. The binning in $p_{\mathrm{T}}^{\mathrm{H}}$ is built in such a way as to ensure that at least 60% of the signal events generated in a given $p_{\mathrm{T}}^{\mathrm{H}}$ bin is also reconstructed in that bin. This procedure yields the following bin boundaries: [0–15 GeV], [15–45 GeV], [45–85 GeV], [85–125 GeV], [125–165 GeV], [165–∞ GeV].

TABLE I. – *Summary of requirements used in the definition of the fiducial phase space.*

Kinematic requirements for the $H \to WW \to 2\ell 2\nu$ fiducial phase space	
Leading lepton p_T	$p_T > 20\,\text{GeV}$
Sub-leading lepton p_T	$p_T > 10\,\text{GeV}$
Pseudorapidity of electrons and muons	$\lvert\eta\rvert < 2.5$
Invariant mass of the two leptons	$m_{\ell\ell} > 12\,\text{GeV}$
Transverse momentum of the lepton pair	$p_T^{\ell\ell} > 30\,\text{GeV}$
Invariant mass of the leptonic system in the transverse plane	$m_T > 50\,\text{GeV}$
No E_T^{miss} cut applied	

4. – Background estimation

The contribution of the dileptonic $t\bar{t}$ production is estimated independently in each p_T^H bin, by measuring the $t\bar{t}$ normalization in a control region enriched in b jets. The control region is orthogonal to the signal region and was obtained requiring at least two jets with $p_T > 30\,\text{GeV}$, one of which characterized by a large value of the b tagging discriminator.

Another important background is nonresonant $WW \to 2\ell 2\nu$. This background is determined independently in each p_T^H bin. The shape of this background in each bin is taken from the simulation, while its normalization is determined from data, owing to the different $(m_{\ell\ell}, m_T)$ shape with respect to the signal contribution.

Backgrounds containing one or two fake leptons are estimated from events selected with relaxed lepton quality criteria, using the techniques described in ref. [8].

The nonegligible contribution from the $Z/\gamma^* \to \tau^+\tau^-$ process is estimated in data replacing $Z/\gamma^* \to \mu^+\mu^-$ events with a simulated $\tau \to \ell\nu_\tau\bar{\nu}_\ell$ decay.

Other less important backgrounds are estimated using simulation.

5. – Systematic uncertainties

Systematic uncertainties and are divided into three categories: uncertainties in background predictions, uncertainties in the experimental measurements and theoretical uncertainties.

Estimation of most of the systematic uncertainties are taken from the $H \to WW \to 2\ell 2\nu$ published analysis [8]. One of the main differences is in the uncertainties related to the prediction of the contributions from $t\bar{t}$ and tW processes. The shapes of those backgrounds are corrected for different b tagging efficiency in data and simulation and the normalization is taken from data in a top-quark enriched control region independently for each p_T^H bin.

The analysis takes into account the theoretical uncertainties that affect the normalization and shape of all backgrounds predicted using simulations and the signal distribution shape. These are uncertainties from the missing higher-order corrections in perturbative QCD, and those related to the PDF uncertainties.

Since the $(m_{\ell\ell}, m_T)$ shape of the WW background contribution is taken from simulation, the corresponding shape uncertainty is estimated comparing different theoretical calculations and including the effect originated from considering different QCD scales.

A summary of the main sources of systematic uncertainty and their contribution is shown in table II.

The uncertainties related to the unfolding procedure are discussed in sect. **7**.

TABLE II. – *Main sources of systematic uncertainty with the associated order of magnitude. The background uncertainties refer to the estimation of the corresponding background. The experimental and theoretical uncertainties refer to the effect on the signal contribution.*

Uncertainties in background contributions	
Source	Uncertainty
$t\bar{t}$, tW	$\sim$ 20–50%
W + jets	$\sim$ 40%
WZ, ZZ	$\sim$ 4%
W$\gamma^{(*)}$	$\sim$ 30%
Experimental uncertainties	
Luminosity	2.6%
Trigger efficiency	1–2%
Lepton reconstruction and ID	3–4%
Lepton energy scale	2–4%
$E_{\mathrm{T}}^{\mathrm{miss}}$ modeling	2%
Jet energy scale	10%
Pileup multiplicity	2%
b mistag modelling	$\sim$ 3%
Theoretical uncertainties	
b jet veto	$\sim$ 1–2%
PDF	$\sim$ 1%
WW shape	$\sim$ 1%

6. – Measured $p_{\mathrm{T}}^{\mathrm{H}}$ spectrum

The signal, including ggH, VBF and VH production mechanisms, is extracted in each bin of $p_{\mathrm{T}}^{\mathrm{H}}$ performing a simultaneous binned maximum likelihood fit in the $m_{\ell\ell}$-m_{T} plane.

Some of the reconstructed H $\rightarrow$ WW $\rightarrow 2\ell 2\nu$ signal events might originate from outside of the fiducial phase space, due to the detector resolution effects. These out-of-fiducial signal events cannot be precisely handled by the unfolding procedure and are subtracted from the measured spectrum. A comparison of data and background prediction is shown in fig. 1, where the $m_{\ell\ell}$ distribution is shown for each of the six $p_{\mathrm{T}}^{\mathrm{H}}$ bins. Distributions are shown inside a m_{T} window of [60, 110] GeV to emphasize the signal contribution.

The spectrum obtained after having performed the fit and after the subtraction of the out-of-fiducial signal events, but before undergoing the unfolding procedure, is shown in fig. 2, where the theoretical prediction of POWHEG V1 after the simulation of the detector is shown for comparison.

7. – Unfolding

To facilitate comparisons to theoretical predictions or other experimental results, the signal extracted performing the fit has to be corrected for detector resolution and efficiency effects and for the efficiency of the selection defined in the analysis. The unfolding procedure in this analysis relies on the Singular Value Decomposition [12] method based on the Tikhonov regularization function.

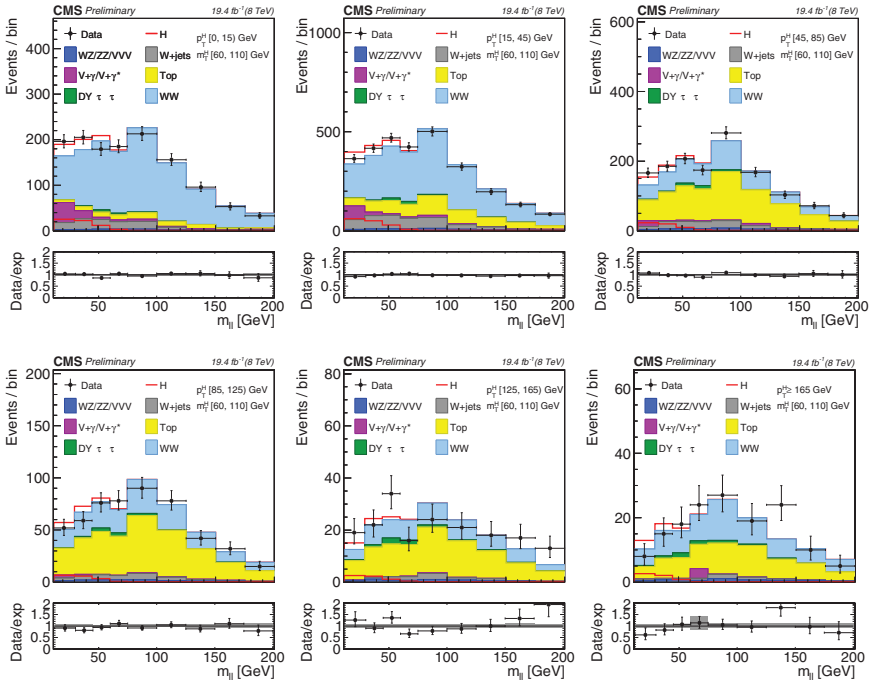

Fig. 1. – Distributions of the $m_{\ell\ell}$ variable in each $p_{\mathrm{T}}^{\mathrm{H}}$ bin. Background normalizations correspond to the estimations obtained from the fit. Signal normalization is fixed to the SM expectation. Ratios of the expected and observed event yields in individual bins are shown in the panels below the plots.

The response matrix was built as a two-dimensional histogram, with the generator level $p_{\mathrm{T}}^{\mathrm{H}}$ on the y-axis and the same variable at reconstructed level on the x-axis, using the same binning for both distributions. The response matrix after normalizing each row to unity is shown in fig. 3.

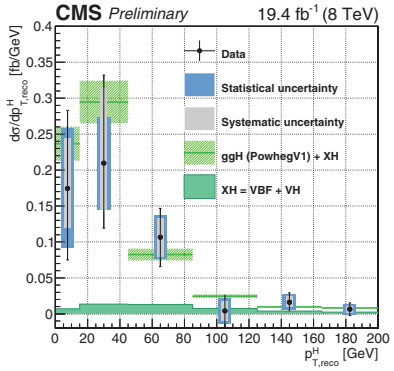

Fig. 2. – Differential Higgs boson production cross section as a function of reconstructed $p_{\mathrm{T}}^{\mathrm{H}}$, before applying the unfolding procedure. Data values are shown together with the statistical (dark azure band) and the systematic (light gray band) uncertainties. The green line and slashed area represent the ggH SM theoretical estimate by POWHEG V1. The sub-dominant component of the signal is denoted as XH = VBF + VH and it is also shown separately.

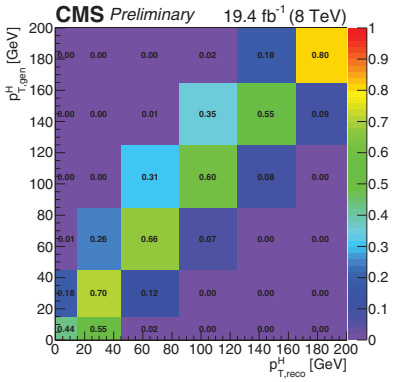

Fig. 3. – Response matrix including all signal processes. The matrix is normalized by row in order to emphasize the resolution effects.

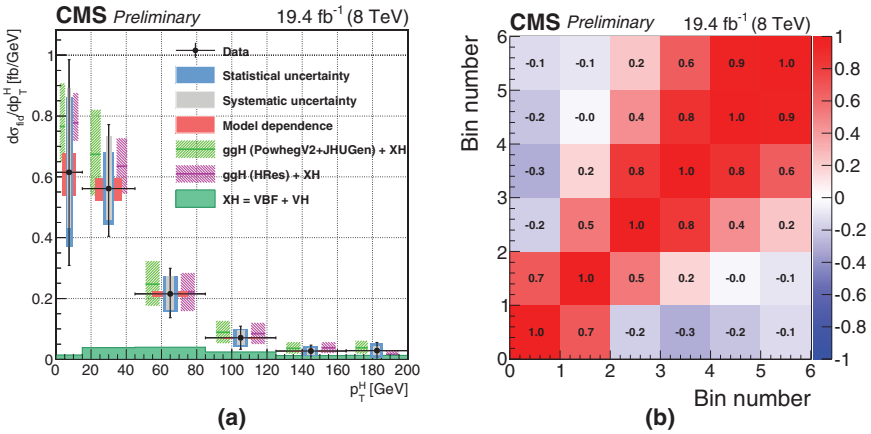

Fig. 4. – (a) Differential Higgs boson production cross section as a function of $p_{\mathrm{T}}^{\mathrm{H}}$, after applying the unfolding procedure. Unfolded data points are shown, together with statistical uncertainty (dark azure band) and systematic uncertainty (light gray band). The vertical bars on the data points correspond to the sum in quadrature of the statistical and systematic uncertainties. The model dependence uncertainty is also shown (dark red band). The pink line and back-slashed area, and the green line and slashed area represent the ggH SM theoretical estimates by HRes and Powheg V2 respectively. The sub-dominant component of the signal is denoted as XH=VBF+VH and it is also shown separately. (b) Matrix of correlations among the $p_{\mathrm{T}}^{\mathrm{H}}$ bins in the unfolded spectrum.

The treatment and the propagation through the unfolding procedure of the systematic uncertainties is performed differently depending on the source of uncertainty. The first source contains the uncertainties that affects only the signal yield, which are handled by the unfolding procedure including the correlations among different $p_{\mathrm{T}}^{\mathrm{H}}$ bins. The second source contains the uncertainties that affect both the signal yield and the response matrix. These are propagate through the unfolding procedure by building different response matrices for each uncertainty. Finally, the third source contains the uncertainties that affect only the response matrix. These are referred to as uncertainties in the signal

model, and are evaluated using a different signal model for building a response matrix, *i.e.* varying the VBF/ggH ratio with respect to the SM.

8. – Results

The unfolded spectrum of $p_{\mathrm{T}}^{\mathrm{H}}$ is shown in fig. 4(a). Statistical, systematic and theoretical uncertainties are shown as separate error bands in the plot. Data are in agreement with the theoretical predictions of HRes and Powheg V2.

Due to the unfolding procedure and to the systematic uncertainties the neighbouring bins in the spectrum have a high level of correlation, as shown in fig. 4(b).

The inclusive fiducial cross section times branching fraction is also measured to be

$$\sigma_{\mathrm{fid}} = 39 \pm 8\ (\mathrm{stat}) \pm 9\ (\mathrm{syst})\ \mathrm{fb}, \tag{2}$$

in agreement within the uncertainties with the theoretical estimate of $48 \pm 8\,\mathrm{fb}$.

REFERENCES

[1] ATLAS Collaboration, *Phys. Lett. B*, **716** (2012) 1.
[2] CMS Collaboration, *Phys. Lett. B*, **716** (2012) 30.
[3] Harlander R. V. and Neumann T., *Phys. Rev. D*, **88** (2013) 074015.
[4] Grazzini M. and Sargsyan H., *JHEP*, **09** (2013) 129.
[5] CMS Collaboration, *Eur. Phys. J. C*, **76** (2013) 13.
[6] CMS Collaboration, *JHEP*, **04** (2016) 005.
[7] CMS Collaboration, *CMS Physics Analysis Summary, CMS-PAS-HIG-15-010* (2015).
[8] CMS Collaboration, *JHEP*, **01** (2014) 096.
[9] Alioli S., Nason P., Oleari C. and Re E., *JHEP*, **04** (2009) 02.
[10] Alwall J., Frederix R., Frixione S., Hirschi V., Maltoni F. *et al.*, *JHEP*, **07** (2014) 079.
[11] Sjöstrand T., Mrenna S. and Skands P., *JHEP*, **05** (2006) 026.
[12] Hocker A. and Kartvelishvili V., *Nucl. Instrum. Methods A*, **372** (1996) 469.